Journal of Power Sources 205 (2012) 93–99

Contents lists available at SciVerse ScienceDirect

Journal of Power Sources

journal homepage: www.elsevier.com/locate/jpowsour

Synthesis of highly dispersed platinum/carbon catalyst using cetyltrimethyl ammonium bromide as a dispersant for proton exchange membrane fuel cells

Rong-Hsin Huang[a], Wen-Kai Chao[a], Ruei-Sung Yu[b], Kan-Lin Hsueh[c,*], Fuh-Sheng Shieu[a,*]

[a] Department of Materials Science and Engineering, National Chung Hsing University, Taichung 40227, Taiwan
[b] Department of Photonics and Communication Engineering, Asia University, Taichung 41354, Taiwan
[c] Department of Energy Engineering, National United University, Miaoli 36003, Taiwan

ARTICLE INFO

Article history:
Received 25 October 2011
Received in revised form
27 December 2011
Accepted 1 January 2012
Available online 20 January 2012

Keywords:
Platinum nanocatalyst
Proton exchange membrane fuel cells
Cetyltrimethyl ammonium bromide
Electrochemically active surface area

ABSTRACT

The highly dispersed platinum/carbon (Pt/C) catalysts with excellent activity were synthesized using an impregnation method with cetyltrimethyl ammonium bromide (CTAB) as a dispersant. The catalysts were then calcined at 300 °C under high vacuum to remove CTAB. The calcination temperature used was lower than the high temperatures (≥500 °C) typically used for removing surfactants in nitrogen or argon. The high vacuum pressure prevents the aggregation and oxidation of Pt nanoparticles. Transmission electron microscopy results showed that the Pt nanoparticles, which had average sizes of 2.0, 2.3, and 2.7 nm at CTAB concentrations of 1.37×10^{-2}, 2.75×10^{-2}, and 4.12×10^{-2} M, respectively, were well dispersed on carbon black. Thermogravimetric analyses indicated that the Pt/C catalysts content increased with increasing CTAB concentration. Cyclic voltammetry analyses confirmed that the electrochemically active surface area and long-term stability of the Pt/C catalysts were better than those of commercial 20 wt.% Pt/C catalyst. The Pt/C-4.12 catalyst performed exceptionally well; the power density of a single cell was 40.9% and 45.4% higher than that of a commercial one at operating cell temperatures of 25 and 75 °C, respectively. The results show that Pt/C catalysts synthesized from this method have promising applications in proton exchange membrane fuel cells.

1. Introduction

Proton exchange membrane fuel cells (PEMFCs), which use hydrogen and oxygen as fuels, have been recognized to be the most promising candidates for a wide range of applications in transportation and home and portable devices [1,2]. PEMFCs have near-zero pollutant emissions, high power density, high energy conversion efficiency, and simplicity of operation that far exceed those of conventional internal combustion systems that use fossil fuels [3–5]. Considerable efforts have been made to commercialize PEMFCs. However, a number of key challenges have yet to be overcome. The Pt utility efficiency of platinum/carbon (Pt/C) catalysts has a direct influence on the performance of PEMFCs [6–9]. A Pt/C catalyst with a high utility efficiency aims to optimize the performance and durability of PEMFCs. Researchers have concentrated on improving the dispersal of Pt nanoparticles on carbon black (CB) to increase the Pt utility efficiency of Pt/C catalysts. An effective dispersion method would not only yield a Pt/C catalyst with a high utility efficiency but also reduce the quantity of Pt used, and thereby reduce the overall cost of producing such catalysts. Various dispersion techniques, such as hydrothermal techniques [10], impregnation [6], sol–gel techniques [11], and the grafting of organics [9,12,13], each of which has been used extensively in the synthesis of nanoparticles, have been proposed. Furthermore, surfactants, such as tetraoctylammonium bromide (TOAB) [14], cetyltrimethyl ammonium bromide (CTAB) [15,16], and 3-(*N*,*N*-dimethyldodecylammonio) propanesulfonate (SB12) [7], which are used to form micelles and prevent the aggregation of nanoparticles, are key components in these dispersion methods. The adsorption of surfactants to the surface of a Pt/C catalyst would greatly reduce its activity. Thus, surfactants must be completely removed to maximize the effectiveness of the Pt/C catalyst, and calcination of the as-synthesized Pt/C catalyst at high temperatures (≥500 °C) [7,14,15] is the conventional approach with which to achieve this. Pt nanoparticles oxidize and aggregate easily at high temperatures with the potential to greatly reduce the utility efficiency of the Pt/C catalyst. In the literature, few studies have focused on the addition of CTAB for the dispersion of Pt nanoparticles on CB (XC-72) to improve the activity of the resulting catalysts. Song et al. prepared Pt/carbon hollow nanospheres catalysts using CTAB as a dispersant [16] that required calcination at 600 °C to remove the surfactant. Zhou et al. reported that CTAB could improve the wettability of mesoporous carbon and the dispersion of Pt nanoparticles [15].

* Corresponding authors. Tel.: +886 4 2285 4563; fax: +886 4 2285 7017.
E-mail addresses: kanlinhsueh@hotmail.com (K.-L. Hsueh), fsshieu@dragon.nchu.edu.tw, D9666210@mail.nchu.edu.tw (F.-S. Shieu).

0378-7753/$ – see front matter © 2012 Elsevier B.V. All rights reserved.
doi:10.1016/j.jpowsour.2012.01.026

In the current study, a commercially and readily available cationic surfactant CTAB was used as a dispersant to enable the excellent dispersal of the Pt/C catalyst. CTAB includes lipophilic alkyl and hydrophilic amine groups that are capable of suspending nanoparticles to form micelles or serve as linkers between the carrier and the metal ion via electrostatic interactions in aqueous solution. A significant attempt was made to reduce the surfactant removal temperature to 300 °C by exploiting the process of vacuum thermal-treatment to enhance the activity of the synthesized Pt/C catalysts. The crystal structure and composition of the as-received Pt/C catalysts were characterized using X-ray diffraction (XRD) and energy dispersive X-ray spectrometry (EDS). The influence of CTAB concentration on both the Pt nanoparticle size and the Pt loading of the Pt/C catalysts was analyzed using transmission electron microscopy (TEM) and thermo-gravimetric analysis (TGA). The formation of well-dispersed Pt nanoparticles and the Pt particle morphology of the Pt/C catalysts were analyzed using TEM and scanning electron microscopy (SEM). The activity and stability of the Pt/C catalysts were demonstrated using cyclic voltammetry (CV). A polarization test was used to investigate the performance of the Pt/C catalysts in the fuel cells. Single cells based on the Pt/C catalysts perform favorably compared with those produced using commercial catalysts (Johnson Matthey, JM-20 wt.%-Pt/C) at operating temperatures of 25 and 75 °C.

2. Experimental

2.1. Preparation of the Pt/C catalyst

The 20 wt.% Pt/C catalysts were synthesized by the impregnation method [6,17]. The method consists of following steps. First, 30 mL of cetyltrimethyl ammonium bromide ($C_{19}H_{42}BrN$, CTAB, Sigma, 99.9%) aqueous solution was prepared in the various concentrations of 4.12×10^{-2}, 2.75×10^{-2}, and 1.37×10^{-2} M. Second, each solution of different concentration was ultrasonically mixed with 1.0 g CB (Vulcan® XC-72, Cabot) for 30 min to obtain finely dispersed CB particles. Third, 0.663 g $H_2PtCl_6{\cdot}6H_2O$ (Alfa Aesar, 99.95%), 10 mL of 1 M NaOH, and 10 mL of methanol (EM-1001, 99.8%, ECHO, Chemical Co., Ltd.) were added to each aforementioned mixture to prepare the good dispersion of Pt/C catalysts using an impregnation method at 80 °C for 4 h. Fourth, the as-made Pt/C catalysts were filtered, washed with 50 mL of alcohol and 200 mL of deionized water, and then dried in a vacuum oven at a pressure of 101.32 Pa under 80 °C for 6 h. Finally, the as-made Pt/C catalysts were calcined in a vacuum oven at a pressure of 1.20 Pa from room temperature to 300 °C. The ripe deliberation of calcination temperature selected was based on the report of Wu et al. [18], who presented the oxidation temperatures of CTAB between 220 °C and 350 °C. Table 1 gives the quantity of CTAB used during the preparation of the Pt/C catalysts.

2.2. Physicochemical characterization of the Pt/C catalyst

The crystal structure of the Pt nanoparticles was analyzed using a MAC MXP III X-ray diffractometer with Cu Kα radiation (λ = 0.154 nm, sweeping angle of 2θ = 10–90°, sweeping rate of $2^\circ\ min^{-1}$), and the diffraction peaks were compared with those in the JCPDS data file. The morphology and distribution of Pt nanoparticles were examined using a field emission scanning electron microscope (FE-SEM, JEOL 6700, Japan) coupled with an X-ray energy dispersive spectrometer (EDS) operating at 15 kV, and a high-resolution transmission electron microscope (HR-TEM, JEOL 2100F, Japan) operating at 200 kV. The weight percentages of the Pt nanoparticles in the Pt/C catalysts were measured using a thermogravimetric analyzer (Perkin Elmer TG/DTA 6300, USA) at temperatures ranging from 25 °C to 800 °C with a 5 °C min^{-1} ramp rate in air. Cyclicvoltammetry (CV), which was used to analyze the electrochemically active surface area (S_{ESA}) of the Pt/C catalysts, was performed under ambient conditions with a scanning rate of 10 mV s^{-1} from −0.3 V to 1.2 V in 1.0 M H_2SO_4 solution, and the long-term stability of the Pt/C catalysts was operated at 0.6 V in 0.5 M H_2SO_4 + 1 M CH_3OH solution using a CHI-614B (CH Instrument, USA) electrochemical analyzer and a standard three-electrode electrochemical cell. Ag/AgCl and a platinum wire were used as the reference electrode and counter electrode, respectively. The working electrode was prepared by coating the surface of a disk-type carbon electrode with Pt/C ink (Zensor R&D Co., Ltd.).

The electrode ink was prepared using 5 mg of Pt/C catalyst ultrasonically suspended with 50 μL of 0.5 wt.% Nafion solution for 1 h. Approximately 10 μL of Pt/C electrode ink was spread onto the surface of a clean standard carbon electrode using a micropipette, and the electrode dried at 80 °C for 1 h in a vacuum oven at a pressure of 1.013×10^3 Pa. The drying process assisted in fixing the Pt/C ink on the carbon electrode, resulting in a thin active layer with a Pt/C loading of 0.51 μg cm^{-2}. The working electrodes were entirely activated to a steady state by 10 cycles in a 0.5 M H_2SO_4 solution at 50 mV s^{-1} using CV prior to the tests. The effective yielding area of the standard carbon electrode was 0.196 cm^2. Table 2 lists the Pt loading of all samples used for CV.

2.3. Measurement of polarization curves

Membrane-electrode assembly (MEA) polarization curves were measured using a fuel cell workstation (Beam Associate Co., Ltd.). The Pt loading on both the anode and cathode was maintained at 0.4 mg cm^{-2}, and the effective area of the MEA was 5 cm^2. A commercial hydrophobic carbon cloth (Beam Associate Co., Ltd.) was used as the gas diffusion layer. Nafion 112 (DuPont) membranes of an area of 4 cm × 4 cm, which was pretreated with 5 wt.% H_2O_2 (Aldrich), deionized water, and 1.0 M H_2SO_4 solution (Aldrich, 98.5%) at 80 °C for 1 h, was used as the separator. Hydrogen and oxygen were provided to both the anode and cathode at a streaming rate of 100 sccm. The performance of the MEA was characterized at a potential sweep rate of 0.56 V min^{-1} at 25 and 75 °C using the fuel cell workstation. The humidifier temperature of both the anode and cathode was maintained at the same temperature as the MEA, and the polarization test was performed under ambient conditions.

3. Results and discussion

3.1. Characterization of the Pt/C catalyst

Fig. 1 shows the wide-angle XRD spectra of the Pt/C catalysts and the commercial 20 wt.% Pt/C catalyst (JM-20 wt.%-Pt/C). As can be seen in the figure, none of the diffraction peaks of CTAB appeared, implying that the CTAB was nearly removed from the synthesized

Table 1
The Pt loadings (wt.%) of the Pt/C catalysts by EDS and TGA.

Catalyst sample	Theoretical loading (wt.%)	The Pt loading (wt.%) by EDS	The Pt loading (wt.%) by TGA
Pt/C-4.12	20	18.76	19.02 ± 0.76
Pt/C-2.75	20	15.88	16.21 ± 0.72
Pt/C-1.37	20	11.36	11.12 ± 0.43

Table 2
The electrochemical characteristics of the Pt/C catalysts.

Catalyst sample	Proportion Pt/C (wt.%)	Particle size (nm)	Pt loadings (mg cm^{-2})	S_{CSA} (m^2 g^{-1})	S_{ESA} (m^2 g^{-1})	Pt utilization efficiency (%)
JM	20	2.8 ± 1.2	0.101	100.13	50.44	50.37
JM[a]	20	3.0 ± 1.2	0.038	93.45	51.30	54.89
Pt/C-4.12	19.02	2.7 ± 1.0	0.096	103.84	65.97	63.53
Pt/C-2.75	16.21	2.5 ± 0.9	0.081	112.14	66.43	59.23
Pt/C-1.37	11.12	2.3 ± 1.0	0.056	121.90	68.02	55.79

[a] JM taken from [26].

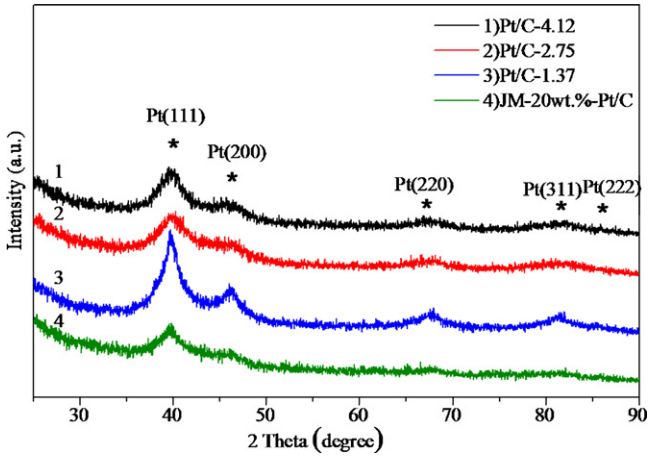

Fig. 1. XRD diffraction patterns of the Pt/C catalysts and commercial catalyst (JM-20 wt.%-Pt/C).

Pt/C catalysts that were calcined at 300 °C. The diffraction peaks of Pt were observed at 2θ values of 39.85°, 46.19°, 67.74°, and 81.52°, corresponding to the crystalline planes of Pt at (1 1 1), (2 0 0), (2 2 0), and (3 1 1), respectively, as compared with the JCPDS data file (No. 04-0802). The XRD results show that the Pt in the catalyst has a face-centered cubic (FCC) structure. Fig. 2 shows FE-SEM images of the Pt/C catalysts. The images show that the spherical morphology of Pt nanoparticles was well dispersed on the surface of carbon black.

Fig. 3 shows the low magnification of the TEM images of Pt/C catalysts, which coincide with the SEM observation, where the Pt nanoparticles were uniformly dispersed on CB. Moreover, the selection area diffraction (SAD) patterns in Fig. 3 (inset) illustrate the FCC structure of the Pt nanoparticles, which is consistent with the XRD results. Fig. 4 shows the HR-TEM images and size histogram of the Pt nanoparticles in the Pt/C catalysts; the average size of the Pt nanoparticles in each sample was found to be 2.8 ± 1.2, 2.7 ± 1.0, 2.3 ± 1.2, and 2.0 ± 1.3 nm, corresponding to JM-20-Pt/C, Pt/C-4.12, Pt/C-2.75, and Pt/C-1.37, respectively. The sizes of the Pt nanoparticles were obtained by directly measuring approximately 400 isolated grains from 50 high-resolution pictures of each sample. The average size of the Pt nanoparticles slightly increased from 2.3 nm to 2.8 nm with increasing quantity of CTAB added to the synthesis solution. This result is similar to the results obtained by Zhou et al. [15].

The high dispersion of the Pt/C catalysts may be attributed to the lipophilic alkyl and hydrophilic amine groups of CTAB. CTAB, CB, and the platinum precursor ($H_2PtCl_6{\cdot}6H_2O$) are mixed in the

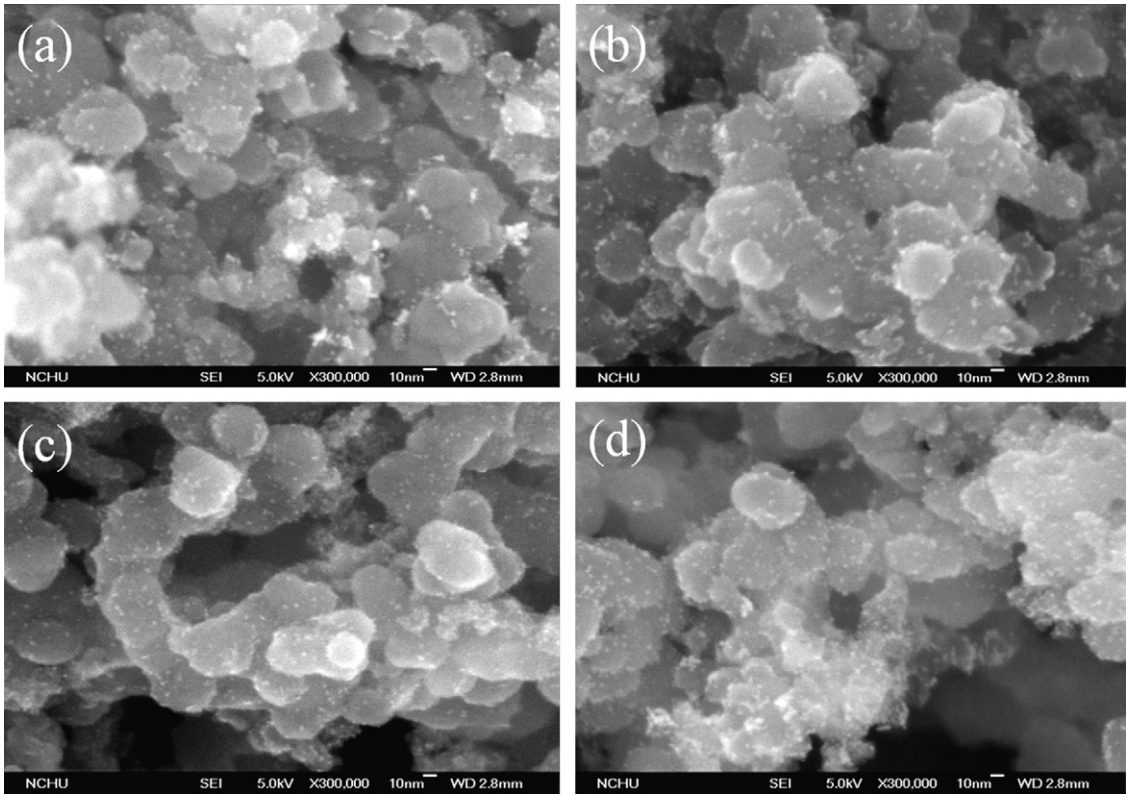

Fig. 2. FE-SEM images of the Pt/C catalysts: (a) JM-20 wt.%-Pt/C, (b) Pt/C-4.12, (c) Pt/C-2.75, and (d) Pt/C-1.37.

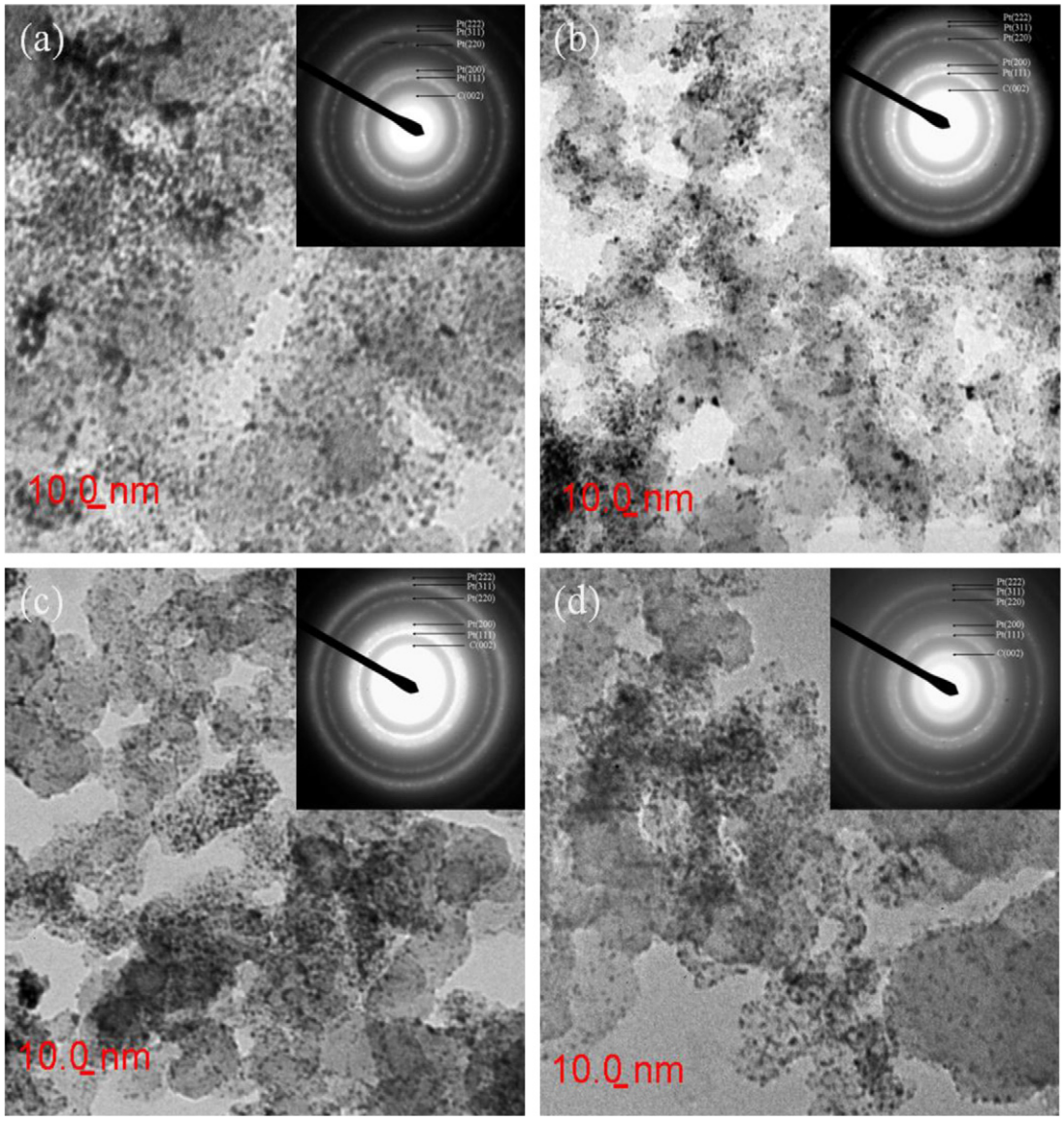

Fig. 3. TEM images of the Pt/C catalysts: (a) JM-20 wt.%-Pt/C, (b) Pt/C-4.12, (c) Pt/C-2.75 and (d) Pt/C-1.37, (inset) the SAD pattern.

aqueous solution. CB is decorated with the hydrophilic amine group to form a micelle, which is suspended and inhibits self-aggregation in the aqueous solution. CTAB also stabilizes the platinum precursor via electrostatic interactions between CTA^+ and $PtCl_6^{2-}$ [15]. The diameter of the spherical Pt nanoparticles was measured using TEM. The chemical surface area (S_{CSA}, $m^2\,g^{-1}$) of the spherical Pt nanoparticles was calculated using the following equation [19,20]:

$$S_{CSA} = \frac{6}{\rho \times d} \quad (1)$$

where ρ is the density of the Pt metal ($21.4\,g\,cm^{-3}$) and d is the average diameter of the metal particles (nm); the results of chemical surface area calculations are shown in Table 2. In the current study, the diameters of the Pt nanoparticles in the Pt/C catalysts were compared with that of the commercial catalyst, and the following order was found: JM-20 wt.%-Pt/C > Pt/C-4.12 > Pt/C-2.75 > Pt/C-1.37; opposite results were obtained for the chemical surface area.

3.2. Pt content in the Pt/C catalyst

The composition of Pt/C catalysts and the Pt mass loading in the Pt/C must be determined before measuring the specific active surface area of the Pt nanoparticles; the necessary information was obtained using EDS and TGA [21,22], respectively. Fig. 5 displays the EDS spectrum of the Pt/C-4.12 catalyst, in which the Pt and C peaks are present. Fig. 6 shows the typical TGA weight loss curves of the catalysts. The results of the EDS and TGA are summarized in Table 1. The proportion of Pt/C measured using TGA was similar to that measured using EDS. Both results show that the Pt content increased with the increasing CTAB concentration. The increase in Pt content is due to the ability of the CTA^+ of the CTAB molecule to attract the $PtCl_6^{2-}$ molecules via electrostatic interactions. The Pt nanoparticles were significantly stabilized and reduced on the surface of CB. The loss of residual Pt nanoparticles can be attributed to the fact that they were not adsorbed onto the surface of CB but were suspended in the ink solution. The loss was then induced by the filtering process of deionized water and alcohol washing. The Pt content of the Pt/C catalysts was determined by the amount

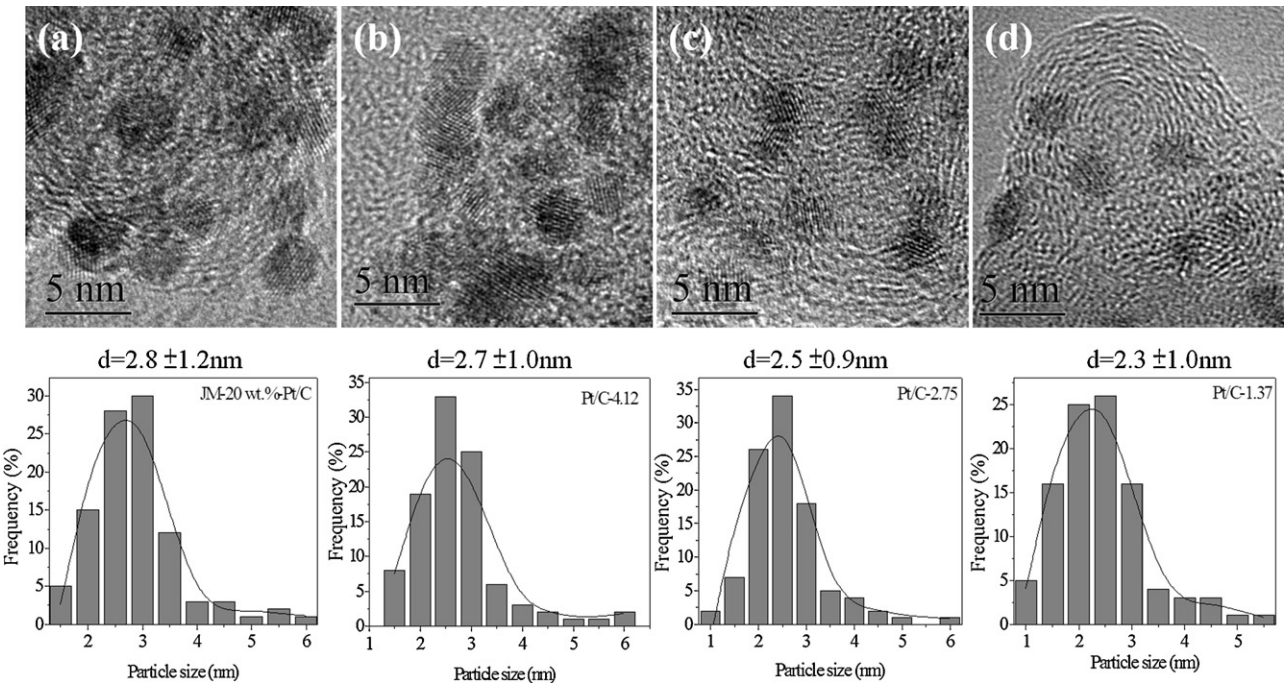

Fig. 4. High-resolution TEM images and size histogram of the Pt/C catalysts: (a) JM-20 wt.%-Pt/C, (b) Pt/C-4.12, (c) Pt/C-2.75, and (d) Pt/C-1.37.

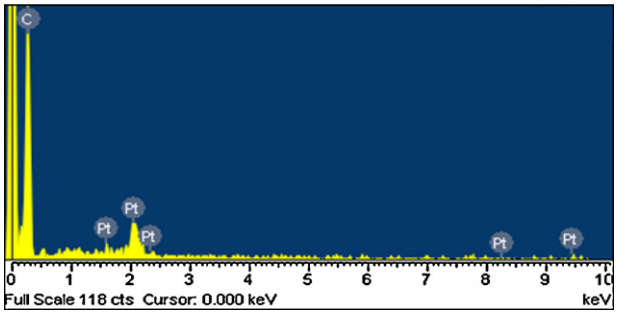

Fig. 5. EDS spectrum of the Pt/C-4.12 catalyst.

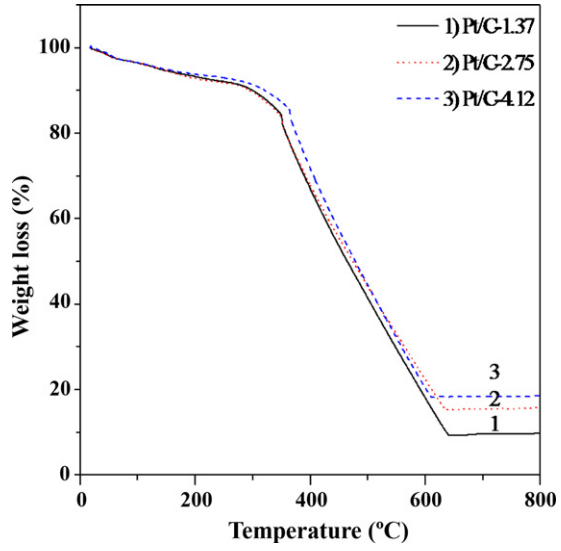

Fig. 6. TGA curves of Pt/C-4.12 (dashed line), Pt/C-2.75 (dotted line), and Pt/C-1.37 (solid line).

of CTAB added. The proportion of Pt in the Pt/C-4.12 catalyst was 19 wt.% ± 0.76 wt.%, which is very close to the theoretical value of 20 wt.%, indicating that a suitable quantity of CTAB addition induces a slight Pt loss. Su et al. [22] reported that the oxidation temperature of XC-72 carbon-based materials occurs in the temperature range between 550 °C and 740 °C; a higher temperature of 800 °C was required in the current experiment.

3.3. Electrochemical characterization of the Pt/C catalyst

A microelectrode technique [23] was used to control the Pt content in the catalytic layer to near or below 0.1 mg cm^{-2} Pt/C. The weight percentage of Pt in each electrode is listed in Table 2. The electrochemical activity area of the catalytic layer with various Pt loadings was estimated from the CV results, as shown in Fig. 7. The hydrogen adsorption–desorption peaks were well defined in

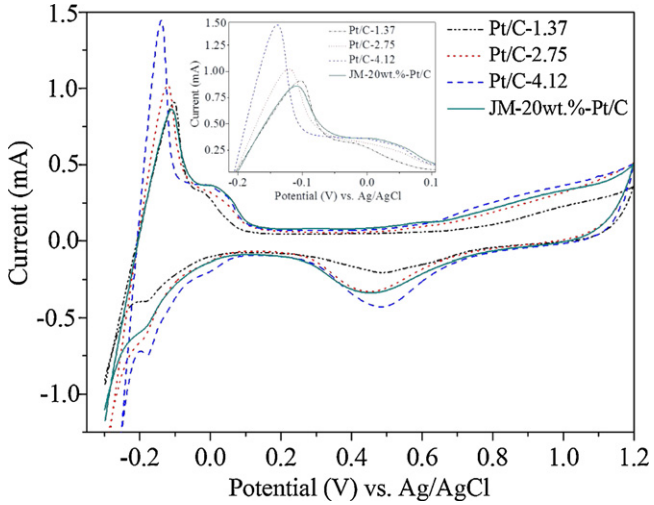

Fig. 7. CV curves of the Pt/C catalysts in 1.0 M H_2SO_4 solution at a scan rate of 10 mV s^{-1}; Pt/C-1.37 (dash dot), Pt/C-2.75 (dot), Pt/C-4.12 (dash), and JM-20 wt.%-Pt/C (solid). The inset image is the hydrogen desorption region of the electrodes.

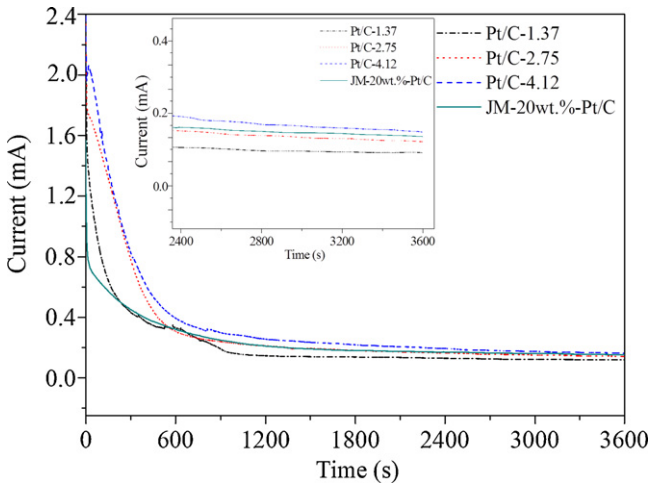

Fig. 8. Chronoamperometric *I–t* curves of the Pt/C catalysts at 0.6 V in 1 M CH_3OH + 0.5 M H_2SO_4 solution. Pt/C-1.37 (dashed-dotted line), Pt/C-2.75 (dotted line), Pt/C-4.12 (dashed line), and JM-20 wt.%-Pt/C (solid line). The current density reaches the steady-state region at ca. 2400–3600 s (inset image).

the potential range from −0.2 V to 0.12 V (inset image). The large specific active area was due to the uniform distribution of the Pt nanoparticles, as demonstrated in the TEM images. The electrochemically active area of the Pt catalyst per unit weight of Pt (S_{ESA}, m^2 Pt mg^{-1} Pt) was calculated based on the quantity of hydrogen desorbed between approximately −0.20 and 0.12 V, as shown in Fig. 7 (inset). S_{ESA} can be calculated using the following equation [8,24,25]:

$$S_{ESA}[m^2\ \text{Pt}\ mg^{-1}\ \text{Pt}] = \frac{(\text{Measured H charge}\ \ (\mu C\ cm^{-2}))/(210(\mu C\ cm^{-2}\ \text{Pt}))}{\text{Pt loading}\ \ (mg\ cm^{-2})} \quad (2)$$

The calculated S_{ESA} results are listed in Table 2. The results show that the specific active area of the Pt/C catalysts increased with decreasing Pt particle size. All the electrodes (labeled Pt/C) have a higher specific active area than the commercial one (labeled JM). The active area of the commercial sample was obtained from data in the literature [26] and was used as a reference. The catalytic utilization of each electrode was calculated using the following equation:

$$\text{Pt utilization efficiency}\ \ (\%) = S_{ESA} \times \frac{100}{S_{CSA}} \quad (3)$$

As can be seen in Table 2, the Pt utilization efficiency of the best sample Pt/C-4.12 was 63.53%, which is 13.16% higher than that of the commercial catalyst.

Fig. 8 shows the stability of the Pt/C catalysts and the typical current–time (*I–t*) curves of the Pt/C electrodes with 0.51 μg cm^{-2} loading at 0.6 V (vs. Ag/AgCl) in 3600 s. The *I–t* curves show that the Pt/C electrode is very stable under the experimental conditions. The current quickly decreased during the first 900 s, and then reached a constant current at around 1200 s. The current remained constant up to 3600 s. As can be seen in the inset of Fig. 8, the steady-state current density of the Pt/C electrodes is in the order of Pt/C-1.37 (2.10) > Pt/C-2.75 (1.74) > Pt/C-4.12 (1.67) > JM-20 wt.%-Pt/C (1.50) A g^{-1} cm^{-2}, which is consistent with the order of active area measured by CV.

3.4. Single cell polarization test

Fig. 9(a) and (b) shows the polarization curves of four different membrane-electrode assemblies (MEAs) at cell temperatures of 25 and 75 °C, respectively. MEA-1, MEA-2, MEA-3, and MEA-JM were prepared with Pt/C-4.12, Pt/C-2.75, Pt/C-1.37, and JM 20 wt.% Pt/C catalysts, respectively. Table 3 shows a list of the open circuit voltage (OCV), maximum current density, and power density of these MEAs. For comparison, the catalytic loading for each electrode was maintained at 0.4 mg cm^{-2}. The same electrode was used as both the anode and cathode during measurement. The cell temperature and humidification temperature of both the anode and cathode were constant in the experiments. Fig. 9(c) and (d) shows the corresponding polarization curves over a small current density region of 0.0–0.3 A cm^{-2}. In this region, the electrochemical activity of the catalyst has a major effect on the polarization curve. As shown in Fig. 9(c) and (d), at 0.6 V, the current density is in the order of MEA-3 > MEA-1 > MEA-2 > MEA-JM at 25 °C and MEA-3 > MEA-2 > MEA-1> MEA-JM at 75 °C. The current density at cell voltages below 0.6 V was mainly affected by ohmic and concentration polarization losses. The current density in voltages below 0.6 V was in the order of MEA-1 > MEA-2 > MEA-3 > MEA-JM at both 25 and 75 °C.

The order of the MEA current density over a small current density (0–0.3 A cm^{-2}) was different from that in a large current density (voltage below 0.6 V) because of two factors, namely, the catalyst utilization and the internal resistance. The slope of the ohmic polarization curves was in the order of MEA-JM > MEA-3 > MEA-2 > MEA-1, as shown in Fig. 9(a) and (b), at 25 and 75 °C, respectively. The in-house MEA (from 1 to 3) had a lower internal resistance than the commercial MEA due to fact that the carbon support used in MEA-1 to MEA-3 had lower electric resistance than that used in the commercial MEA. The utilization efficiency of the Pt/C catalysts in the small current density region appeared to be a much more important factor than the internal resistance in influencing the current density. In the current density region used, MEA-1 to MEA-3 showed lower activation losses than the commercial one.

Overall, MEA-1 had the highest power density among all the MEAs. MEA-1 had a power density of 0.37 W cm^{-2} or 0.937 W cm^{-2} mg^{-1} at 25 °C, which is 40.9% higher than that of MEA-JM. At 75 °C, the maximum power density of MEA-1 is 45.4% higher than that of the commercial one. The other MEAs also showed better performance than the commercial one at both temperatures. The results above indicate that the proper combination

Table 3
The open circuit voltage, current density, and power density of various membrane electrode assemblies.

Operation temperature (°C)	MEA sample	Pt/C catalyst	Open circuit voltage initial (V)	Maximum current density (A cm^{-2} mg^{-1})	Maximum power density (W cm^{-2} mg^{-1})
25–25–25	MEA-JM	JM-20 wt.%	0.820	3.805	0.665
	MEA-1	Pt/C-4.12	0.855	5.167	0.937
	MEA-2	Pt/C-2.75	0.864	4.652	0.827
	MEA-3	Pt/C-1.37	0.874	4.567	0.882
75–75–75	MEA-JM	JM-20 wt.%	0.831	3.815	0.620
	MEA-1	Pt/C-4.12	0.826	5.292	0.902
	MEA-2	Pt/C-2.75	0.833	5.195	0.910
	MEA-3	Pt/C-1.37	0.879	4.555	0.857

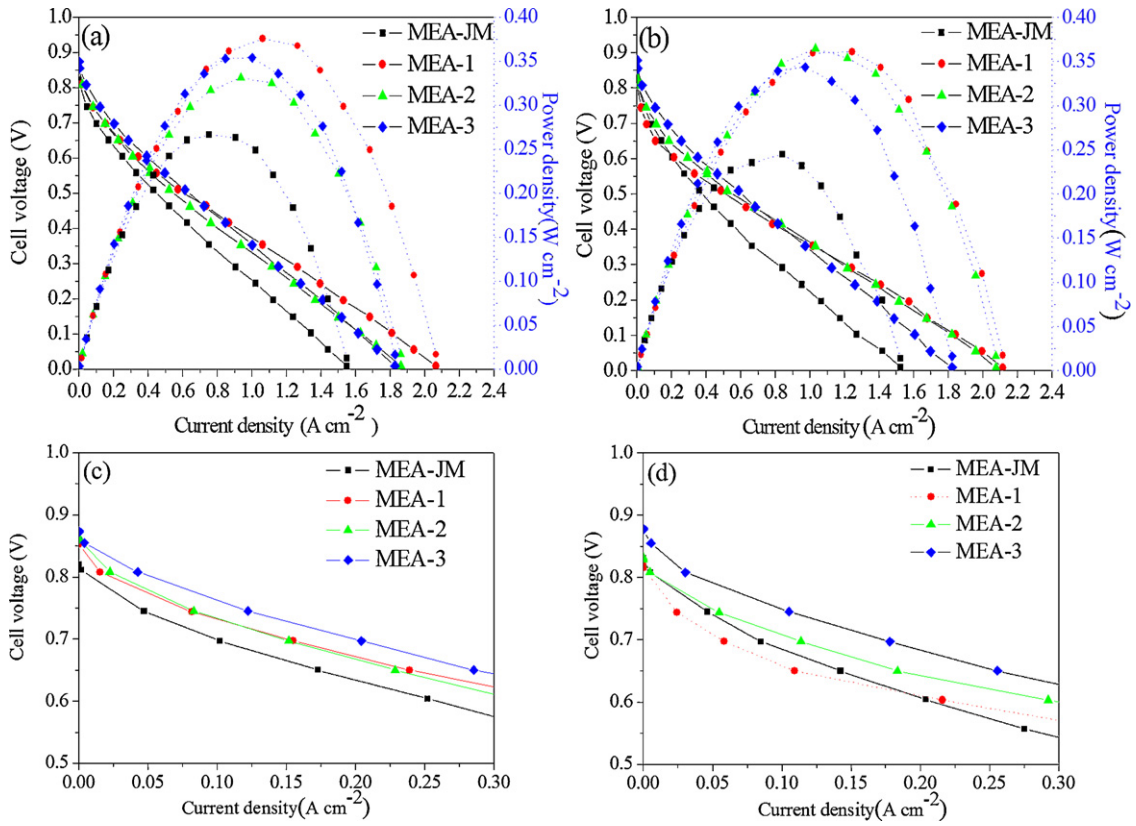

Fig. 9. Polarization curves of the MEAs measured at operating temperatures of (a) 25 °C and (b) 75 °C; (c) and (d) the corresponding polarization curve plots in the small current density region from 0.0 to 0.3 A cm^{-2} at 25 °C and 75 °C, respectively.

of small Pt particle size, uniformity of catalyst distribution, and Pt/C composition best improves MEA performance. The Pt/C-4.12 catalyst and its MEA showed exceptional performance.

4. Conclusion

This study developed an easy and efficient method of synthesizing well-dispersed and highly active Pt/C catalysts using the surfactant CTAB, which serves as a dispersant, via a 300 °C vacuum calcination process. The thermal-treatment process significantly assisted in the removal of the surfactant, and the Pt/C catalysts exhibited outstanding functionality. The Pt diameter and the Pt content of the Pt/C catalysts increased with increasing CTAB concentration. The large area and distinct peaks obtained from the hydrogen adsorption–desorption analyses demonstrate that the well-dispersed Pt nanoparticles in the Pt/C catalysts have excellent electrocatalytic activity. The steady-state *I*–*t* curves show that the Pt/C catalysts have long-term stability under the experimental conditions employed in this study. The resulting polarization curve demonstrates that the significant electrocatalytic capability of the prepared Pt/C catalysts by this method can be exploited in a fuel cell environment.

Acknowledgments

The authors would like to thank the National Science Council of the Republic of China, Taiwan, for financially supporting this research under Contract No. NCS-97-2221-E-005-016-MY3. Ted Knoy is appreciated for his editorial assistance.

References

[1] K.B. Prater, J. Power Sources 61 (1996) 105.
[2] D.O.J. Murphy, G.D. Hitchens, D.J. Manko, J. Power Sources 47 (1994) 353.
[3] R. Beneito, J. Vilaplana, S. Gisbert, Int. J. Hydrogen Energy 32 (2007) 1544.
[4] J. Chen, T. Matsuura, M. Hori, J. Power Sources 131 (2004) 155.
[5] G. Hoogers, Fuel Cell Technology Handbook, CRC Press, Boca Raton, FL, 2003.
[6] Y.H. Pai, J.H. Ke, C.C. Chou, J.J. Lin, J.M. Zen, F.S. Shieu, J. Power Sources (2006) 398.
[7] C.L. Hui, X.G. Li, I.-M. Hsing, Electrochim. Acta 51 (2005) 711.
[8] S. Song, Y. Wang, P.K. Shen, J. Power Sources 170 (2007) 46.
[9] P. Yu, M. Pemberton, P. Plasse, J. Power Sources 144 (2005) 11.
[10] C. Kim, M. Noh, M. Choi, J. Cho, B. Park, Chem. Mater. 17 (2005) 3297.
[11] W.F. Yan, S.M. Mahurin, Z.W. Pan, S.H. Overbury, S. Dai, J. Am. Chem. Soc. 127 (2005) 10480.
[12] H. Spinelli, Adv. Mater. 10 (1998) 1215.
[13] J. Yu, N. Grossiord, C.E. Koning, J. Loos, Carbon 45 (2007) 618.
[14] J. Prabhuram, X. Wang, C.L. Hui, I.M. Hsing, J. Phys. Chem. B 107 (2003) 11057.
[15] J.H. Zhou, J.P. He, Y.J. Ji, W.J. Dang, X.L. Liu, G.W. Zhao, C.X. Zhang, J.S. Zhao, Q.B. Fu, H.P. Hu, Electrochim. Acta 52 (2007) 4691.
[16] Y.Y. Song, Y. Li, X.H. Xia, Electrochem. Commun. 9 (2007) 201.
[17] W.K. Chao, C.M. Lee, S.Y. Shieu, C.C. Chou, F.S. Shieu, J. Power Sources 185 (2008) 136.
[18] S. Han Wu, D.H. Chen, J. Colloid Interface Sci. 273 (2004) 165.
[19] S.G. Song, Y. Wang, P.K. Shen, J. Power Sources 170 (2007) 46.
[20] J. Zeng, J.Y. Lee, W. Zhou, Appl. Catal. A: Gen. 308 (2006) 99.
[21] M. Chen, Y.C. Xing, Langmuir 21 (2005) 9334.
[22] F. Su, J. Zeng, X. Bao, Y. Yu, J.Y. Lee, X.S. Zhao, Chem. Mater. 17 (2005) 3960.
[23] F. Maillard, M. Martin, F. Gloaguen, Electrochim. Acta 47 (2002) 3431.
[24] G. Tamizhmani, J.P. Dodelet, D. Guay, J. Electrochem. Soc. 143 (1996) 18.
[25] W. Li, W. Zhou, H. Li, Z. Zhou, B. Zhou, G. Sun, Q. Xin, Electrochim. Acta 49 (2004) 1045.
[26] H.Q. Li, G.Q. Sun, N. Li, S.G. Sun, D.S. Su, Q. Xin, J. Phys. Chem. C 111 (2007) 5605.